TÜBİTAK

Turkish Journal of Chemistry

http://journals.tubitak.gov.tr/chem/

Research Article

Turk J Chem
(2017) 41: 773 – 783

doi:10.3906/kim-1701-54

Palladium nanoparticles entrapped in melamine-formaldehyde resin microparticles for Mizoroki–Heck reactions

Shaofeng ZHONG*
Department of Textiles, Zhejiang Industry Polytechnic College, Shaoxing, P.R. China

Received: 22.01.2017 • **Accepted/Published Online:** 05.05.2017 • **Final Version:** 10.11.2017

Abstract: Melamine-formaldehyde resin (MFR) microparticles with average diameters of 1.06 μm were synthesized with PEG-20000 as the particle-forming agent. Palladium nanoparticles were entrapped in and adsorbed on the MFR microparticles, consecutively. Scanning electron microscopy (SEM) was used to characterize the morphologies of MFR microparticles. X-ray diffraction (XRD) and transition electron microscopy (TEM) showed that the palladium nanoparticles entrapped in the MFR microparticles dispersed much more homogeneously than those adsorbed on the MFR microparticles. Mizoroki–Heck reaction catalysis results demonstrated that the entrapped palladium catalyst had similar catalytic activity with the adsorbed palladium catalyst. Moreover, this novel entrapped palladium catalyst could be reused at least for 10 times without obvious loss of initial activities and with only 6.5% of overall palladium leaching.

Key words: Palladium, melamine-formaldehyde resin, Mizoroki–Heck reaction, entrap, heterogeneous

1. Introduction

Palladium catalysts play an important role in organic synthesis and pharmaceutical and polymer chemistry.[1,2] Palladium and various ligands have been synthesized and widely used in homogeneous catalysis for their high selectivity and efficiency. However, homogeneous palladium catalyst suffers the problems of separation, recovery, and regeneration of the palladium catalyst and the pollution of products and the environment.[3] Heterogeneous palladium catalyst is an efficient way to overcome these limitations. However, due to the disfavored kinetics of the biphasic catalytic system, the heterogeneous catalyst was generously not as active as homogeneous catalyst. Thus, in order to increase the collision between the palladium species with the substrates, palladium species were usually anchored on the surface of supporting solid matrices with larger specific surface area.[4–8] Moreover, in order to decrease the leaching of palladium in catalysis and increase the activities of supported catalysts, solid matrices were usually chemical modified with various chelating ligands to enhance the interaction between the solid matrices with palladium.[9–11] However, it is still a great challenge to avoid the leaching of palladium species from the supporting matrices as the interaction between the supporting matrices with palladium species would be weakened in harsh reaction conditions, such as high reaction temperature.

Recently, palladium species have been entrapped in ionic liquid microgel,[12] sol-gel materials,[13] and nanofiber mat,[14,15] which exhibited high catalytic activity and stability for the C–C coupling reaction. These results demonstrate that palladium species entrapped in supporting matrices would be an efficient way to avoid the leaching of palladium by the interception of a crosslinked polymer chain. However, it is still very difficult

*Correspondence: sfzhong@163.com

to prepare heterogeneous palladium catalyst with both high activity and low leaching of palladium. In the present study, heterogeneous palladium catalyst with high activity and stability was successfully prepared by entrapping palladium species in melamine-formaldehyde resin microparticles (Figure 1).

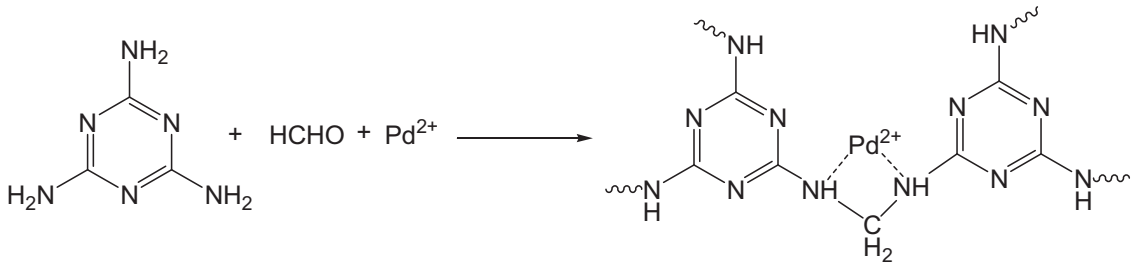

Figure 1. Schematic representation for the synthesis of melamine-formaldehyde resin supported palladium catalyst (Pd@MFR).

2. Results and discussion

2.1. Characterization of the catalysts

Melamine-formaldehyde resin (MFR) has excellent physical and chemical stability, and is widely used in industry.[16,17] As MFR contains a lot of secondary and tertiary amine groups, which could chelate with metal ion effectively, MFR has great potential in heavy metal removal and heterogeneous transition metal catalyst preparation. As shown in Figure 2, the absorption bands at 1552, 1492, 1341, and 814 cm^{-1} were assigned to C=N, $-CH_2-$, C–N, and triazine ring, respectively, which clearly proved the successful synthesis of MFR. However, due to the small amount of palladium, the Pd-MFR (palladium nanoparticles adsorbed on the MFR particles) and Pd@MFR1 (palladium nanoparticles entrapped in the MFR particles) had the same FT-IR spectra as that of MFR (Figure 2).

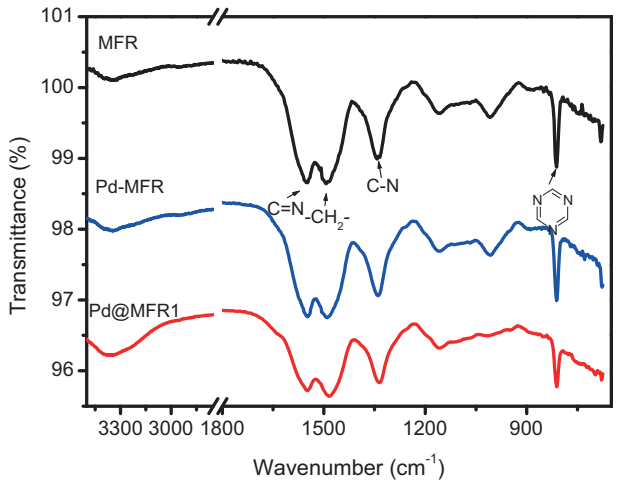

Figure 2. FT-IR spectra of MFR, Pd-MFR, and Pd@MFR1.

As we known, MFR is very difficult to prepare as microparticles as it is crosslinked quickly in the polymerization procedure. Herein, with 2 g of PEG-20000 as the particle forming agent, well-defined MFR particles were synthesized and then used to immobilize the palladium catalyst (Pd-MFR, average diameter =

1.01 ± 0.28 μm) (Figures 3A and 3B). By addition of palladium ion in the MFR synthesis procedure, palladium-entrapped MFR (Pd@MFR1) microparticles were prepared with average diameter of 1.08 ± 0.23 μm (Figures 3C and 3D), which is a little larger than that of Pd-MFR microparticles. Moreover, the BET analysis showed that the surface area of Pd-MFR was 3.15 m^2/g, while that of Pd@MFR1 was 2.07 m^2/g. Thus, it can be concluded that the interaction of palladium ion with MFR would lead to the increment of average diameter and decrement of surface area of MFR microparticles. By decreasing the amount of PEG-20000 to 0.5 g, the average diameter of palladium-entrapped MFR particles (Pd@MFR2) increased to 10.31 ± 4.49 μm (Figures 3E and 3F). Thus, it can be concluded that the size of MFR particles could be adjusted by the amount of PEG-20000. SEM-EDX characterization demonstrated that the palladium nanoparticles were dispersed homogeneously on the MFR particles (Figures 4A–4C).

Besides the SEM-EDX characterization, the dispersions of palladium nanoparticles on MFR microparticles were further analyzed by XRD and TEM (Figures 5 and 6). The three diffraction peaks at 2θ angles of 40°, 47°, and 68° belong to the face centered cubic (FCC) palladium, which are the (111), (200), and (220) planes of the palladium crystal (Figure 3).[18,19] It can be found that the diffraction peaks of Pd@MFR were obviously weaker than these of Pd-MFR, indicating the much more homogeneous dispersion of palladium in Pd@MFR1. TEM images clearly showed that the palladium nanoparticles in Pd@MFR1 were dispersed homogeneously (Figure 6A) while the palladium nanoparticles clusters were found on the Pd-MFR (Figure 6B). The palladium nanoparticle distribution analysis showed that the average diameter of palladium nanoparticles in Pd@MFR1 was 2.77 ± 0.81 nm (Figure 7A), while the average diameter of palladium nanoparticles in Pd-MFR was 6.66 ± 0.81 nm (Figure 7B). Thus, it can be concluded that the crosslinked MFR polymer chain could indeed inhibit the growth and aggregation of palladium nanoparticles.

The swelling capacities of MFR microparticles in DMAc and DMSO solvents were measured. It was found the swelling capacity of MFR in DMAc was larger than that in DMSO (Table 1).

Table 1. The swelling capacities of MFR microparticles.

Solvent	Swelling (g/g)
DMAc	5.55 ± 0.35
DMSO	4.23 ± 0.26

2.2. Catalytic performance of MFR-supported palladium catalysts

In order to increase the contact probability of palladium species with substrates, the palladium species were usually anchored on the surface of supporting matrices with larger specific area.[4–8] As the interaction of palladium species with supporting materials would be greatly decreased at high reaction temperature, it was very difficult to decrease the leaching of palladium species in harsh reaction conditions. Herein, palladium species were entrapped in the supporting materials to decrease the palladium leaching.

The catalytic activities of palladium adsorbed on and entrapped in MFR particles were evaluated by the Mizoroki–Heck reactions (Figure 8). Although the palladium species were entrapped in the MFR particles, the catalytic activity of Pd@MFR1 catalyst was only a little lower compared with the Pd-MFR catalyst. However, the reaction rate was significantly decreased with Pd@MFR2 as the catalyst. These results clearly demonstrated that the particle size of supporting matrices played an important role in the catalytic activity of entrapped palladium catalyst. DMSO and DMAc have been proved to be good solvents for Mizoroki–Heck reactions.[14,15,20] However, it was found that the catalytic activity of Pd@MFR1 in DMSO was not as active as

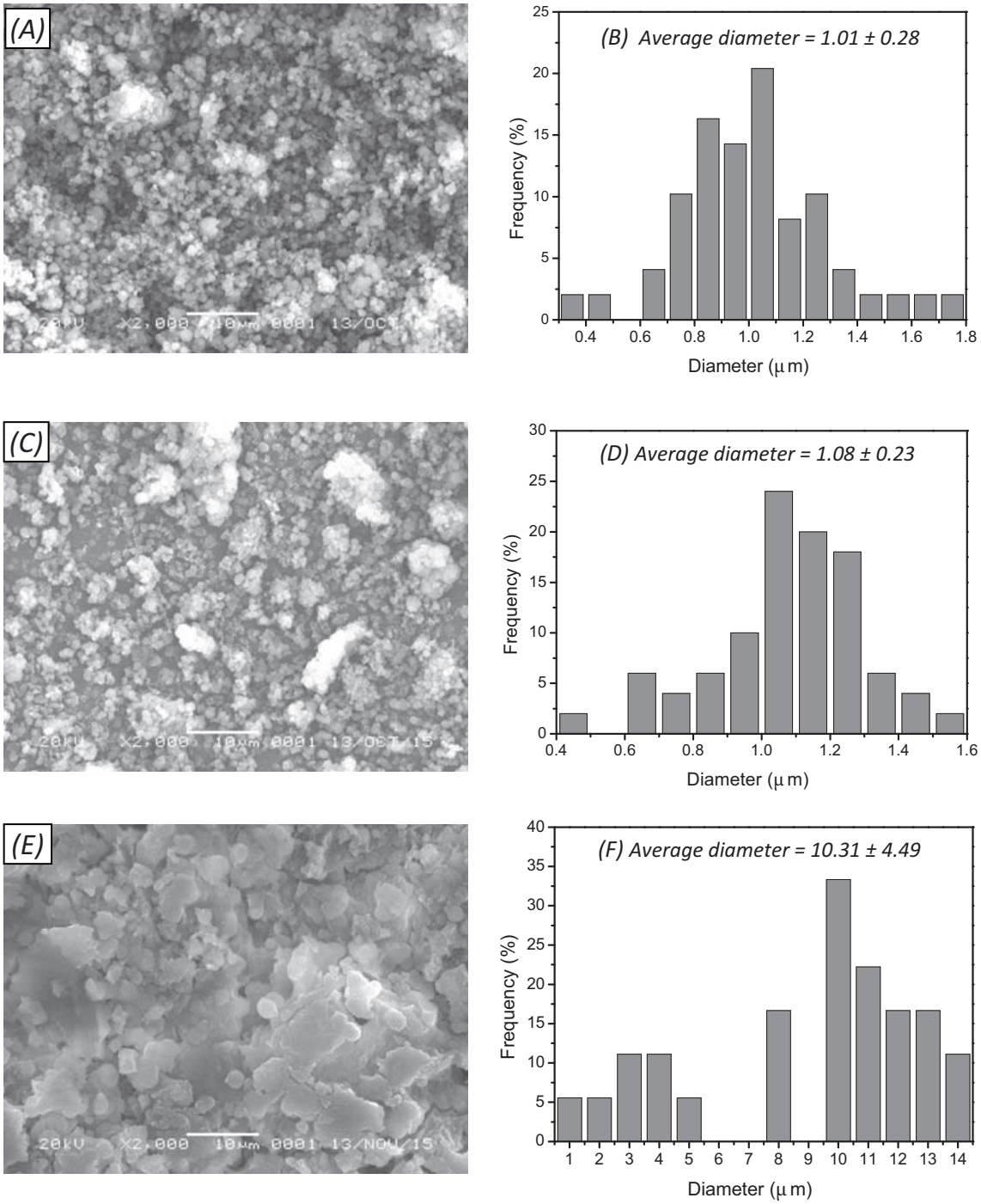

Figure 3. SEM images and the corresponding particle diameter distributions of Pd-MFR (A, B), Pd@MFR1 (C, D), and Pd@MFR2 (E, F).

that in DMAc. As we know, there are a lot of small pores (free volume) in the polymer matrices. We think that these small pores in the MFR matrices allowed the entrance of substrates into the MFR matrices to contact with the palladium species. The swelling results demonstrated that the swelling capacity of MFR particles in DMAc was larger than that in DMSO, which in turn would make the pores of MFR in DMAc larger than those

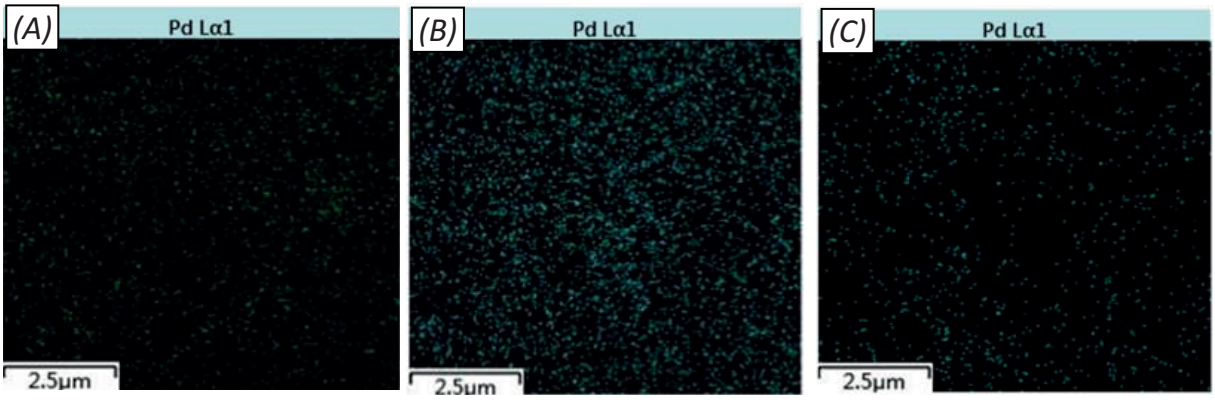

Figure 4. SEM-EDX images of Pd-MFR (A), Pd@MFR1 (B), and Pd@MFR2 (C).

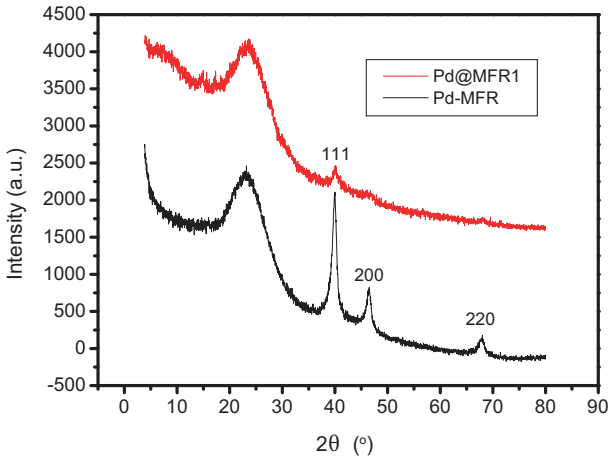

Figure 5. XRD patterns of Pd-MFR and Pd@MFR1.

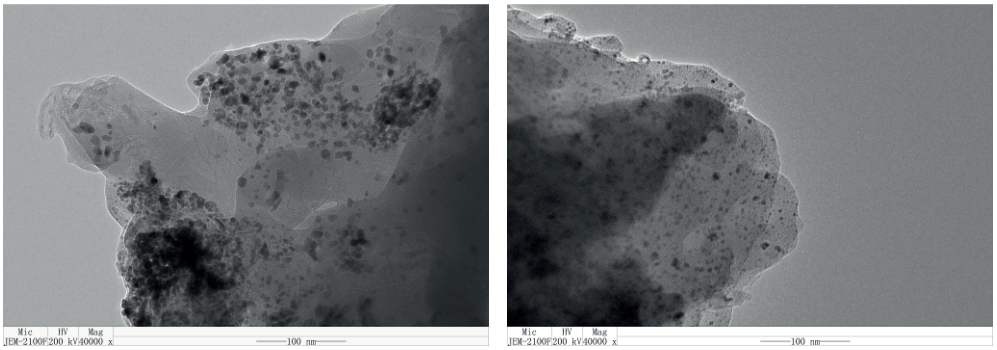

Figure 6. TEM images of Pd-MFR and Pd@MFR1.

in DMSO. As a result, the substrates and products would circulate more easily in MFR matrices in DMAc solution. Thus, it can be concluded that small particle size and high swelling ratio of supporting matrices could facilitate the circulation of substrates in the matrices, which made the internal palladium species active in the catalysis procedure.

A hot filtration experiment was carried out to verify the heterogeneity of Pd@MFR1 in DMAc and DMSO solution. The Pd@MFR1 catalysts were removed from reaction mixtures after reacting for 90 min. The

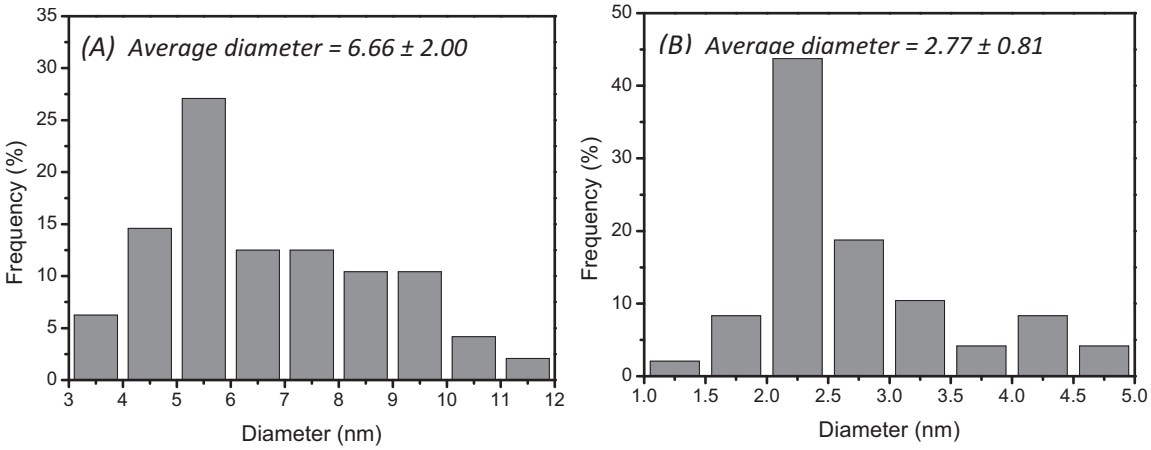

Figure 7. Palladium nanoparticle diameter distributions for (a) Pd-MFR and (b) Pd@MFR1.

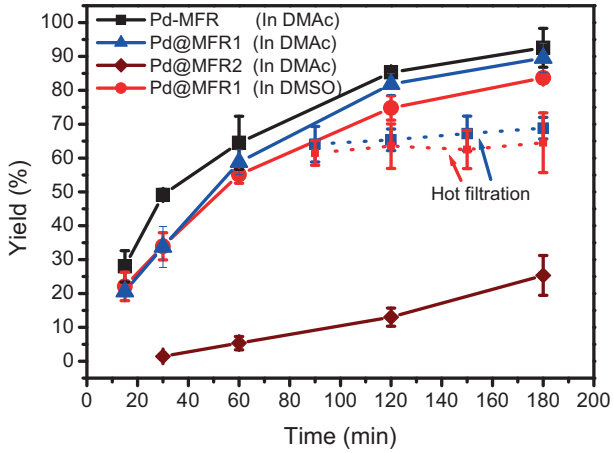

Figure 8. Catalytic comparison of Pd-MFR, Pd@MFR1, and Pd@MFR2 in DMAc and DMSO solution towards the Mizoroki–Heck reaction of iodobenzene with n-butyl acrylate. (Reaction conditions: 16 μmol palladium catalyst, 0.7 mmol iodobenzene, 1.4 mmol n-butyl acrylate, and 5.25 mmol triethylamine in 3.0 mL of DMSO at 110 °C. Yields were determined from the GC-MS measurements based on the amount of iodobenzene.)

GC/MS analysis showed no increment in the yield (Figure 8). The filtrates from DMAc and DMSO solutions were further analyzed by ICP-AES and there was no leaching of palladium, indicating that the reactions proceeded in a heterogeneous fashion.[21–23] Hence, it can be concluded that entrapment of palladium species in the melamine formaldehyde resin structure could increase its stability in the reaction process.

The reusability of Pd@MFR1 in DMAc and DMSO was examined (Figure 9). The result showed that the yield dropped at the sixth run with DMAc as the solvent while the Pd@MFR1 could be reused at least 10 times in DMSO solution without obvious decrement of yield. The palladium content analysis in the recovered Pd@MFR1 catalysts showed that the overall palladium leaching of Pd@MFR1 in DMSO after being reused for 10 cycles was only 6.5%, which was much lower than that in DMAc after being reused for 7 cycles (36.5%). The SEM image of the recovered Pd@MFR1 particles after being reused for 10 cycles showed that the morphology of Pd@MFR1 particles was well kept (Figure 10A) and the average diameter of Pd@MFR1 particles increased to 1.33 ± 0.46 μm from 1.08 ± 0.23 μm (Figure 10B). This result demonstrated that the Pd@MFR1 was very stable to catalyze the Mizoroki–Heck reaction in DMSO solution.

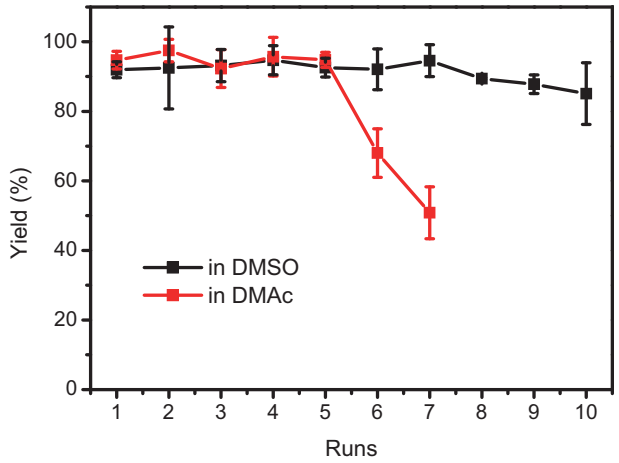

Figure 9. The reuse of Pd@MFR1 in DMSO and DMAc solution. (Reaction conditions: 16 μmol palladium catalyst, 0.7 mmol iodobenzene, 1.4 mmol n-butyl acrylate, and 5.25 mmol triethylamine in 3.0 mL of DMSO at 110 °C. Yields were determined from the GC-MS measurements based on the amount of iodobenzene.)

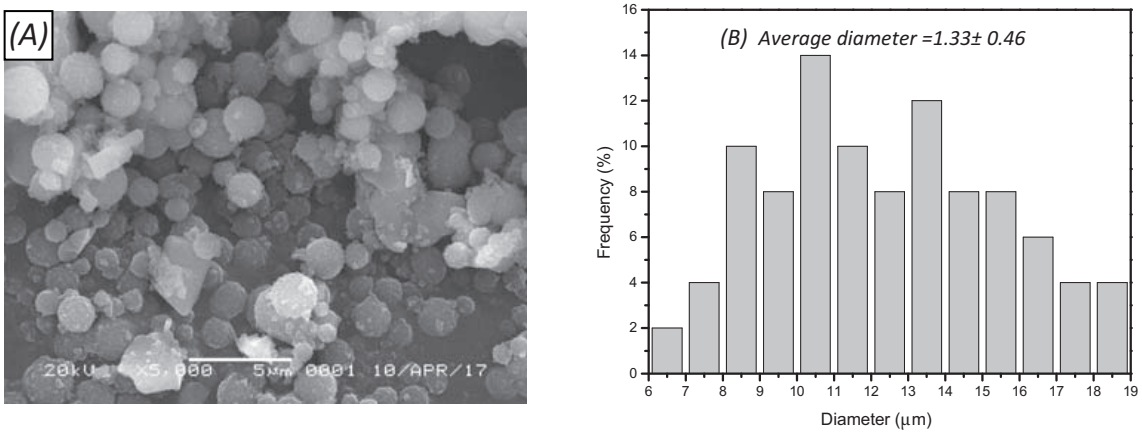

Figure 10. SEM image of Pd@MFR1 after reused for 10 cycles and the corresponding particle diameter distribution.

The Pd@MFR1 was employed to catalyze the Mizoroki–Heck reactions of several representative aromatic halides with alkenes (Table 2). It can be found that the Pd@MFR1 was not very active to catalyze the Mizoroki–Heck reactions of the aromatic iodides with substitute groups at the *ortho*- or *meta*-position or with larger substitute groups due to the high steric hindrance (entries 2, 4, 7, 8, 9, and 10 in Table 2). For the same reason, the aromatic iodides with substitute groups at the *para*-positions acted more efficiently than those with substitute groups at the *ortho*-position (entries 2, 3, 4, 5, and 6 in Table 2). The alkene of styrene was not as active as methylacrylate and $n-$butyl acrylate (entries 1, 11, and 12 in Table 2). These results clearly demonstrated that the steric hindrance of substrate was an important reason responsible for the catalytic activity of Pd@MFR1 catalyzed Mizoroki–Heck reaction of aromatic iodides with alkenes. Fortunately, excellent yields could be obtained with longer reaction time for the examined aromatic iodides and alkenes. However, the Pd@MFR1 has low activity for bromobenzene with n-butyl acrylate, due to the greater strength of the carbon–bromine bond (entry 13 in Table 2).

Table 3 summarizes the dependence of the Mizoroki–Heck reaction with the Pd@MFR1 catalyst loading. We found that the yield for the Mizoroki–Heck reaction of iodobenzene with n-butyl acrylate generally increased

Table 2. Pd@MFR1 catalyzed Mizoroki–Heck reactions of aromatic iodides with acrylates.[a,b]

Entry	Aromatic Iodides	Yield (%, 3 h)	Yield (%, 10 h)
1	PhI	94	95
2	2-FPhI	77	96
3	4-FPhI	81	98
4	2-BrPhI	88	95
5	4-BrPhI	94	95
6	4-ClPhI	96	96
7	4-NO_2PhI	63	92
8	2-CH_3PhI	65	95
9	3-CH_3PhI	75	96
10	4-CH_3OPhI	64	90
11	PhI[c]	92	95
12	PhI[d]	62	86
13	PhBr	5	21

[a]Reaction conditions: 16 μmol Pd@MFR1 catalyst, 0.7 mmol aromatic iodides, 1.4 mmol n-butyl acrylate unless otherwise specified, and 5.25 mmol triethylamine in 3.0 mL of DMSO at 110 °C.
[b]Mizoroki–Heck reaction yields were determined from the GC-MS measurements based on the amount of aromatic iodides substrate.
[c]The acrylate was methacrylate.
[d]The acrylate was styrene.

with the catalyst loading. Although the yields were poor with PhI/Pd ratio over 88 and reaction time of 3 h, the yields could be increased by prolonging the reaction time to 10 h.

Table 3. The effect of added amount of Pd@MFR1 catalyst on the yield of Mizoroki–Heck reactions.[a,b]

Entry	Catalyst amount (mg)	PhI/Pd ratio	Yield (%, 3 h)	Yield (%, 10 h)
1	50	44	94	95
2	35	63	79	92
3	25	88	53	89
4	10	219	29	88

[a]Reaction conditions: 0.7 mmol iodobenzene, 1.4 mmol n-butyl acrylate, and 5.25 mmol triethylamine in 3.0 mL of DMSO at 110 °C.
[b]Mizoroki–Heck reaction yields were determined from the GC-MS measurements based on the amount of iodobenzene.

In summary, well-defined MFR particle-supported palladium catalyst was synthesized with PEG-20000 as the particle-forming agent. Palladium nanoparticles were dispersed homogeneously in MFR microparticles, which showed high catalytic performance towards the Mizoroki–Heck reaction of aromatic iodides with acrylates. Overall, we provided an efficient method to prepare an active and stable heterogeneous transition metal catalyst.

3. Experimental

3.1. Materials

Melamine and formaldehyde aqueous solution (36%) were purchased from Sinopharm Chemical Regent Co. Ltd (Shanghai, China). Aromatic iodides, acrylate, and poly(ethylene glycol) (M_n = 20,000) (PEG-20000) were

bought from Aladdin Industrial Co. Ltd (Shanghai, China). $PdCl_2$ was bought from Hangzhou Changqing Chemical Industrial Co. Ltd (Zhejiang, China).

3.2. Synthesis of melamine-formaldehyde resin (MFR) nanoparticles

Melamine (1,3,5-triazine-2,4,6-triamine, 1.6 g) and PEG-20000 (2.0 g) were added to 3.8 g of formaldehyde aqueous solution (formaldehyde content: 1.0 g) in the presence of hexamethylenetetramine (7.0 mg). The mixture was reacted at 90 °C for 1.5 h. After completion, the mixture was centrifuged and washed with hot water repeatedly to remove the PEG-20000.

3.3. Swelling capacity of MFR particles

The MFR particles were immersed in DMSO or DMAc solution for 48 h and then collected under reduced pressure through a sintered filter funnel (pore size: 3 $\sim$ 4 μm). The swelling capacity of the MFR particles was calculated by the following equation:

$$Q = \frac{m_2 - m_1}{m_1} \tag{1}$$

where m_1 and m_2 are the mass of the dried and swollen MFR particles, respectively. The Q value was calculated as grams of solvent soaked per gram of mat sample.

3.4. Preparation of MFR particles supported palladium catalyst

Palladium entrapped in MFR particles (Pd@MFR): $PdCl_2$ (10 mg) and NaCl (7.0 mg) were dissolved in 1.0 g of H_2O and then some amount of PEG-20000 was added and stirred to get a homogeneous and viscous solution. The melamine (1.6 g), formaldehyde aqueous solution (2.8 g, formaldehyde content: 1.0 g), and hexamethylenetetramine (7.0 mg) were added to the $PdCl_2$/PEG-20000 solution. The mixture was reacted at 90 °C for 1.5 h. After completion, the Pd@MFR was separated by centrifugation and washed with hot water repeatedly to remove the PEG-20000. The synthesized Pd@MFR was added into 5.0 mL of aqueous solution and then 0.1 mL of hydrazine was added to reduce the Pd^{2+} to Pd^0. After 2 h, the Pd@MFR particles were separated by centrifugation and washed with H_2O. The Pd@MFR particles were then dried at 80 °C under reduced pressure for 12 h. The catalyst synthesized with 2.0 g of PEG-20000 was named Pd@MFR1, while the catalyst synthesized with 0.5 g of PEG-20000 was named Pd@MFR2. The inductively coupled plasma-atomic emission spectroscopy (ICP-AES) characterization results showed that the palladium contents in Pd@MFR1 and Pd@MFR2 were both 3.4 wt.%.

The process for the synthesis of palladium adsorbed on MFR particles (Pd-MFR) was as follows: $PdCl_2$ (10 mg) and NaCl (7.0 mg) was dissolved in 5.0 mL of H_2O and then MFR particles (2.0 g) were added to yellow $PdCl_2$ aqueous solution. After 2 h, the solution became colorless, indicating the complete adsorption of Pd^{2+} ion. Next 0.1 mL of hydrazine was added and the mixture was stirred for another 2 h. The solid matrices became completely black, indicating the reduction of Pd^{2+} to Pd^0. The posttreatment was the same as that of Pd@MFR1. ICP analysis showed that the palladium content in Pd-MFR catalyst was 3.2 wt.%.

3.5. General procedure for the Mizoroki–Heck reaction

MFR-supported Pd catalyst (16 μmol) was added to 3.0 mL of DMSO solution containing aromatic iodides (0.7 mmol), acrylate (1.4 mmol), and triethylamine (5.25 mmol) in a 25-mL tubular reactor. The mixture was

stirred magnetically. The reaction was monitored by thin layer chromatography (TLC) and was analyzed by GC/MS. After completion, the reaction was stopped by addition of 10 mL of water. The mixture was then extracted three times with ethyl acetate (3 × 20 mL) and the solvent was removed by rotary evaporator. The crude product was dried under reduced pressure and purified by chromatography on silica gel with a mixture of petroleum ether and ethyl acetate as eluent to afford the corresponding coupling product.

3.6. Reuse of the Pd catalyst

The palladium catalysts were recovered from the reaction media by centrifugation and then were reused for the next run directly.

3.7. Characterizations

The quantitative analysis of the Mizoroki–Heck reaction product was determined by Agilent GC/MS (Agilent, GC6890/5975 MSD, USA). The injector-port and detector temperature was set at 270 °C and the oven temperature was initially set at 80 °C and ramped up to 220 °C at 5.0 °C min^{-1}, and maintained at 220 °C for 2.0 min. The structure of the Mizoroki–Heck reaction product was determined by ^{1}H NMR in $CDCl_3$ with TMS as the internal standard (Bruker, Avance III 400 MHz, Switzerland). The surface morphologies of the catalyst were characterized by scanning electron microscopy (SEM) (Jeol, jsm-6360lv, Japan), while the dispersion of palladium nanoparticles was analyzed by energy dispersive X-ray (EDX) spectrometer (Hitachi, S-4800, Japan), high-resolution transmission electron microscopy (TEM) (Jeol, JEM-2100F, Japan), and X-ray diffraction (XRD) (Empyrean, PANalytical, Netherlands). FT-IR/ATR spectra were recorded on a FT-IR spectrometer (Nicolet, Nexus-470, USA) with the accessories of attenuated total reflection. Inductively coupled plasma-atomic emission spectroscopy (ICP-AES) analysis was performed on a Leeman ICP-AES Prodigy XP (Leeman Labs, USA). The average diameters of MFR and palladium particles were determined from the corresponding SEM and TEM images.

Acknowledgment

We greatly appreciate the financial support from Shaoxing Science and Technology Plan Project (2015B70014) and Zhejiang ?Industry Polytechnic College.

References

1. Phan, N. T. S.; Van Der Sluys, M.; Jones, C. W. *Adv. Synth. Catal.* **2006**, *348*, 609-679.
2. Astruc, D. *Inorg. Chem.* **2007**, *46*, 1884-1894.
3. Glasnov, T. N.; Findenig, S.; Kappe, C. O. *Chem. Eur. J.* **2009**, *15*, 1001-1010.
4. White, R. J.; Luque, R.; Budarin, V. L.; Clark, J. H.; Macquarrie, D. J. *Chem. Soc. Rev.* **2009**, *38*, 481-494.
5. Durap, F.; Metin, Ö. *Turk. J. Chem.* **2015**, *39*, 1247-1256.
6. Wang, G. W.; Kundu, D.; Uyama, H. *J. Colloid Interf. Sci.* **2015**, *451*, 184-188.
7. Barakat, T.; Rooke, J. C.; Franco, M.; Cousin, R.; Lamonier, J. F.; Giraudon, J. M.; Su, B. L.; Siffert, S. *Euro. J. Inorg. Chem.* **2012**, *2012*, 2812-2818.
8. Tamami, B.; Nowroozi Dodeji, R.; Ghasemi, S. *Turk. J. Chem.* **2015**, *39*, 880-885.
9. Sharma, S.; Rajesh, N. *Chem. Eng. J.* **2016**, *283*, 999-1008.

10. Farjadian, F.; Hosseini, M.; Ghasemi, S.; Tamami, B. *RSC Adv.* **2015**, *5*, 79976-79987.
11. Veisi, H.; Hamelian, M.; Hemmati, S. *J. Mol. Catal. A: Chem.* **2014**, *395*, 25-33.
12. Zhang, Y. M.; Quek, X. Y.; Wu, L. L.; Guan, Y. J.; Hensen E. J. *J. Mol. Catal. A: Chem.* **2013**, *379*, 53-58.
13. Reetz, M. T.; Dugal, M. *Catal. Lett.* **1999**, *58*, 207-212.
14. Shao, L. J.; Ji, W. X.; Dong, P. D.; Zeng, M. F.; Qi, C. Z.; Zhang, X. M. *Appl. Catal. A: Gen.* **2012**, *413-414*, 267-272.
15. Shao, L. J.; Liu, J.; Ye, Y. H.; Zhang, X. M.; Qi, C. Z. *Appl. Organometal. Chem.* **2011**, *25*, 699-703.
16. Shao, L. J.; Xing, G. Y.; Qi, C. Z. *Chem. Pap.* **2014**, *68*, 983-988.
17. Yao, Y.; Zhang, B. Q.; Shi, J. Y.; Yang, Q. H. *ACS Appl. Mater. Interf.* **2015**, *7*, 7413-7420.
18. Kim, S.; Lee, D. W.; Lee, K. Y. *J. Mol. Catal. A: Chem.* **2014**, *391*, 48-54.
19. El-Hout, S. I.; El-Sheikh, S. M.; Hassan, H. M. A.; Harraz, F. A.; Ibrahim, I. A.; El-Sharkawy, E. A. *Appl. Catal. A: Gen.* **2015**, *503*, 176-185.
20. Shao, L. J.; Ren, Y.; Wang, Z. N.; Qi C. Z.; Lin, Y. *Polymer* **2015**, *75*, 168-177.
21. Rangel Rangel, E.; Maya, E. M.; Sánchez, F.; de la Campa J. G.; Iglesias M. *Green Chem.* **2015**, *17*, 466-473.
22. Kantam Lakshmi, M.; Srinivas, P.; Shiva Kumar, K. B.; Trivedi, R. *Catal. Commun.* **2007**, *8*, 991-996.
23. Oliveira, R. L.; Hooijmans, J. B. F.; de Jongh, P. E.; Gebbink, R. J. M. K.; de Jong, K. P. *ChemCatChem* **2014**, *6*, 3223-3230.